TEST DATA OF FLOW FIELD OF SHUTTLE SRM NOZZLE JOINT WITH BOND DEFECTS, USING UNHEATED AIR*

Leroy M. Hair
Micro Craft, Inc.

James V. McAnally
Huntsville Sciences Corp.

John E. Hengel
NASA Marshall Space Flight Center
Huntsville, AL

ABSTRACT

The nozzle-to-case joint on the Shuttle SRM (as redesigned after the Challenger accident) features an adhesive sealant filling and bonding the joint, with a wiper o-ring to prevent the adhesive from reaching and disabling the closure o-ring. Flawless implementation of that joint design would ensure that hot, corrosive propellant combustion gases never reach the closure o-ring. However, understanding the flowfield related to bonding defects is prudent. A comprehensive test program was conducted to quantify such flowfields and associated heating environments. A two-dimensional, full-scale model represented 65 inches of the nozzle joint, using unheated air as the test medium, in a blowdown mode. Geometry variations modeled RSRM assembly tolerances, and two types of bonding defects: pullaways and blowholes. A range of the magnitude of each type defect was tested. Also a range of operational parameters was tested, representative of the RSRM flow environment, including duplication of RSRM Mach and Reynolds numbers.

Extensive instrumentation was provided to quantify pressures, heat rates, and velocities. The resulting data established that larger geometric defects cause larger pressure and larger heating, at the closure o-ring region. Velocity trends were not so straight-forward. Variations in assembly tolerances did not generally affect flowfields or heating. Operational parameters affected flowfields and heating as might be expected; increasing density or velocity increased heating. Complete details of this test effort and presented in Ref. 1.

1. INTRODUCTION

Even before the Shuttle 51-L failure of the SRM field joint, the nozzle-to-case joint had been considered an area needing improvement, and a hot-firing ground test program instituted. After 51-L and in conjunction with the RSRM development, an unheated air flow ground test element was added. RSRM nozzle joint details are sketched in Fig. 1. Important features are: (1) an adhesive sealant bonding the outboard rubber-like insulators to the inboard phenolic insulators; (2) a wiper o-ring, to prevent that adhesive from reaching the closure o-ring; and (3) addition of radially-aligned bolts, to minimize the joint spreading due to motor pressure.

Flawless implementation of the joint design will ensure that propellant combustion gases never reach the closure o-ring. However, understanding the flowfield in the presence of bonding defects is prudent. The primary concern is that circumferential flow or pressure gradients along the bonded joint could induce circumferential flow along the closure o-ring, potentially leading to o-ring damage. Such circumferential flow in the nominally-axisymmetric motor case could be caused by nozzle gimballing or by unsymmetrical propellant or inhibitor burning (Refs. 2-4).

A comprehensive test program was performed to quantify the nozzle joint flow associated with bonding defects. The fundamental objective was to define both the flowfield and heating environment in the adhesive slot and in the region between wiper and closure o-rings, due to various sizes and shapes of bonding imperfections, for a range of RSRM operational flow conditions. A secondary objective was to establish a data base suitable for evaluating those computational fluidynamic analytical models which might be used in making flight predictions.

The test program comprised blowdown runs from a 6,000 cu.ft. supply tank, through a full-scale two-dimensional representation of a 65-inch-long segment of the RSRM nozzle joint. Unheated air was the test medium, facilitating extensive instrumentation in the model. Flight values of joint Reynolds No. and Mach No. were achieved. Analysis had indicated that RSRM joint-face velocities might be around Mach = 0.10; this test provided a range from 0.03 - 0.15. RSRM Reynolds No. at Mach = 0.10, at normal combustion temperature and pressure, would be $2-3 \times 10^6$/ft; this test provided a range from $1.5-3.0 \times 10^6$/ft.

This program was denoted "SRM D MSFC 23" by the RSRM project, and AFS-0003 by the MSFC facility. A total of 550 runs were accomplished. Table I presents a capsule of the design test conditions. Details of the apparatus, test operations, and results are given in the next three sections.

2. APPARATUS

BASIC MODEL

The basic model was a two-dimensional (2-D) full-scale representation of a 65-inch section of the SRM Nozzle-to-Case Joint, Fig. 2. Air was supplied to the model via an axisymmetric entrance bellmouth within the test facility's 16-inch diameter feed line. Air exited the model into a plenum and then through a choked, axisymmetric nozzle into the facility exhaust duct.

The 65-inch length and the 3.214-inch diameter bore were chosen primarily to match the geometry of hot-firing tests at Morton Thiokol. Analysis has indicated that circumferential flow might occur over about 120° of SRM joint arc. The 65-inch model length represented about 60% of such a full-scale 120° arc. Model cross-section perpendicular to the axisymmetric bore represented the flight RSRM hardware at ignition, from the entrance/face of the bonded joint, to the closure o-ring position. The closure o-ring was modeled to the nominal installed flight dimensions, using rubber. The wiper o-ring was modeled as being completely compressed into its groove, using metal. If this wiper in fact were at full dimensions, then no propellant gas would reach the closure o-ring vicinity, obviating concern for its integrity.

The modular model system accommodated a variety of 2-D slot geometry configurations, instrumentation packages, and flow control devices. Five exit nozzles were provided, to control bore entrance Mach No. (M_b) to be either 0.03, 0.05, 0.07, 0.10, or 0.15. Five tapered liners were provided for the bore to produce a linear variation of dP/dX along the bore, with overall exit-to-entrance diameter ratios of 0.5, 0.6, 0.7, 0.8, and 0.9. The design values of dP/dX, non-dimensionalized by entrance plenum total pressure (P_o) depended on M_b, Table I.

The basic model was built of aluminum, of left and right halves (Fig. 3 Section A-A) joined using steel bolts, and having stainless steel entrance bellmouth, exit nozzles, and attachment flanges. The tapered bore liners were fiberglass, built up over steel mandrels.

DEBOND MODELS

Two basic types of bonding defects were modeled. The full-length defect where the bonding material pulls away from one of the insulators was modeled at four values of the pullaway distance, Fig. 3a. With the maximum value of 0.100 inches, the classic pre-51L vented joint design was represented. To produce these geometry changes, 65-inch long stainless steel shims were used to position a relocatable element in the slot geometry. The defect where two blow-holes connect the closure o-ring vicinity to the motor combustion chamber was modeled at four values of the blow-hole length (Fig. 3b): 0.5, 1.0, 2.0, and 4.0 inches. Rubber fillers of appropriate length and 0.100 inch thickness were inserted in the slot, to produce these geometry changes and simultaneously form a seal.

ASSEMBLY TOLERANCE MODELS

Five configurations were provided of the slot geometry in closest proximity to the closure o-ring, Fig. 4. These configurations represent either possible mis-matches due to stack-up of tolerances on RSRM hardware, or variation at different locations on the joint circumference. To produce these changes, brass shim stock was used to

position a relocatable element in the wiper-to-closure o-ring land area, plus three different thickness items of slot-to-wiper-o-ring approach geometry were used.

INSTRUMENTATION

The results reported in this paper are from pressure, heat rate, and velocimeter instrumentation, Fig. 5. Six identical planes of comprehensive pressure instrumentation were spaced along the model length, comprising 3 Pitots and 15 statics. Pressures were measured on small-range differential transducers to maximize sensitivity. Relatively low flow velocities were expected, for which Pitot-static data might have a large error band. Moreover, the small slot width gave concern about a practical-sized Pitot, and about Pitot-to-Pitot interference down the 65-inch slot length. Thus only a limited number of Pitots were provided, and hot-wire velocimeters were incorporated to corroborate the Pitot-static data, documented in Ref. 5.

Five planes of three calorimeters each were interdigitated among the pressure stations. Four more calorimeters were positioned in the blow-holes. An unconventional approach was adopted for heat transfer testing. The available facility was not capable of providing heated air, and the model was too complex to contemplate heating it uniformly. Instead, a small area of the model immediately adjacent to each calorimeter was heated (by electrical resistance). This concept had been proven on an earlier test (Ref. 34) with a single calorimeter, and adopted for the 19 calorimeters associated with the reported test. The selected calorimeters had a 5 Btu/(ft^2-s-°F) range.

A comprehensive surface flow visualization phase preceded the reported quantitative data phase, using pigment-doped oil. This qualitative data defined the slot flow due to end effects at the entrance and exit, documented in Ref. 1. A limited exploratory use of laser doppler velocimeters was performed after the primary test, not yet documented.

3. OPERATIONS

The independent parameters in this test were the model geometry (Figs. 3,4) and three operational variables: bore-entrance Mach No. (M_b), bore-entrance Reynolds No. (Re), and bore pressure gradient (dP/dX). M_b was controlled by the exit nozzle area. Re was controlled by the combination of M_b and P_o, the facility stagnation pressure. dP/dX was controlled by M_b, P_o, and the tapered liner exit-to-entrance-diameter ratio, d/d. Figure 6 shows this test equipment could simultaneously match both M_b and Re of the RSRM. The matrix of test conditions investigated is shown in Table 1.

The facility operated in blowdown mode. Desired P_o was established in the supply tank, then the tank valve was opened. At 60 psia, P_o decreased about 0.1 psi/s. Typical runs were about 30 seconds.

DATA REDUCTION

Pressure and temperature data were reduced by standard means. Pressure results were non-dimensionalized to P_o, to account for P_o decreasing during a blowdown run. Hot wire velocimeter data was reduced by special means detailed in Ref.5. Calorimeter data was reduced generally as sketched in Fig. 7. However, two factors required an extensive post-test analysis to produce the results shown below: (1) the determination of slot boundary layer recovery factors, and (2) correcting for wall temperature mismatch, due to the small extent of heated model as compared to the total model. Documenting of these factors was beyond the scope of this paper, but are presented in Ref. 1.

BASIC PERFORMANCE

A test goal was to impress a linear variation of slot entrance pressure along the bore. The tapered liners had been analytically designed to do so. Figure 8 shows that the liners met this goal, for two typical cases, and also presents the associated variation of local bore Mach No. for the case of primary interest with entrance M_b-0.10, dP/dX precisely matched the design value. For the off-nominal case of M_b=0.15, dP/dX was quite linear but less than desired.

PROBE-TO-PROBE INTERFERENCE

Two types of interference were investigated: (1) Pitot-to-Pitot pneumatic, and (2) calorimeter to calorimeter heating. Figure 9 shows that neither concern was significant. It appears that the magnitude of the pneumatic disturbance may have been fairly consistent (between having only one probe, versus having six in line), but was only about 0.1 psia, which is near the lower limit of resolution. Similarly for heat rate, the single-probe data is about 3% different than the data for five calorimeters in line.

4. RESULTS

Results are shown as the effects of the various independent parameters, upon the axial variation of the flowfield and heating environment parameters: P, V_g, and h_g.

EFFECT OF RSRM ASSEMBLY TOLERANCES

The effect upon flowfield and heating was quite small, as shown for limit cases of assembly tolerances in Fig. 10. Generally, no coherent trends were evident among the three different assembly tolerance configurations, so Fig. 10 simply shows bands of data. These band widths are about the same value as instrumentation accuracy, in all cases. Thus it is evident that assembly tolerances do not significantly affect either static pressure, velocity, nor heating in the gap region immediately adjacent to the closure o-ring.

EFFECT OF PULLAWAY DEFECTS

Vertical Variation. Before considering the overall pullaway effect, inspecting the vertical (along the slot) variation is instructive: Figs. 11-12. It is apparent that both static and total pressures are essentially constant along the slot depth. Some end effects are noticeable in the static pressure data. But for the majority of the model length, pressure variations along the slot depth are less than 0.1 psi, which is about the level of data system accuracy. Bore pressure is quite constant.

The variations in heat transfer coefficient along the slot depth is significant. Heating at the gap region immediately adjacent to the closure o-ring is higher than elsewhere. Moreover the vriation of heating along the depth is not the same for the two different pullaway widths.

Gap parameters are of the greatest interest to closure o-ring environment. Thus, the remainder of the pullaway defect discussion will use only gap data.

Pullaway Width. Figure 13 shows the effect of pullaway width, at nominal values of operational parameters. The general result is that the wider pullaway causes higher static pressure and higher heating. However, the velocity data is mixed. In fact most of the velocity data is within the instrumentation accuracy band. Thus it could be concluded that pullaway width has little distinguishable effect on gap velocity.

Operational Parameters. The effects of all three operational parameters are shown in Figs. 14-16. The Re variation presented in Fig. 14 was achieved by varying stagnation pressure. Thus dP/dX also changed even though dP/dX - P_o was constant. Qualitative results are as would be expected: heating increases with Re, for either pullaway width.

The Mach No. variation presented in Fig. 15 was produced at constant stagnation pressure. Thus Re also varied, as did dP/dX - P_o (Table I). Results are -- like Re sensitivity -- as expected: heating increases with air speed. Note that while the non-dimensionalized velocity is quite independent of M_b, the denominator V_b increases linearly with M_b. Thus V_g also increases essentially linearly with M_b.

The dP/dX variation presented in Fig. 16 was produced at constant P_o and M_b, thus Re was also constant. Again, qualitative results are as might be expected: heating increases with gap velocity, as induced by bore pressure differential.

For all three operational parameters just discussed, the conclusions are valid over the majority of the model length. However, in the entrance and exit regions, end effects mute the sensitivity to those operational terms.

EFFECT OF BLOW-HOLE DEFECTS

Significant vertical variation of flowfield and heating environments would be expected for the local entrance and exit blow-hole regions. And there was insufficient instrumentation in the region between wiper and closure o-rings to define any vertical variation, along the model length between blow-holes. Thus data similar to Figs. 11-12 was not available for blow-hole defects.

Blow-hole Length. Figure 17 shows the effect of blow-hole length at nominal values of operational parameters. The general result is that the longer the blow-hole, the higher the static pressure and heating. As with pullaways, the velocity data for blow-holes is mixed. Most of the velocity data for liner $d/d= 0.80$ is within the instrumentation accuracy band. For the more extreme liner $d/d= 0.50$ case, it appears that most blow-hole lengths above 1.0 inch have similar velocity trends, noticeably higher than for smaller blow-hole length.

Operational Parameters. The effects of M_b and dP/dX are shown in Figs. 18-19. As for the pullaway data, the Mach No. variation in Fig. 18 was produced at constant stagnation pressure, so Re and $dP/dX - P_o$ also varied. Heating increases directly with air speed. As opposed to the pullaway case, the blow-hole non-dimensionalized velocity depends strongly (and inversely) on M_b. Thus dimensional velocity is more nearly constant (for varying M_b) with blow-holes, than with pullaways.

The dP/dX variation presented in Fig. 19 was produced at constant P_o and M_b, thus Re was also constant. Qualitative results were as might be expected: heating increases with gap velocity, as induced by bore pressure differential.

As for pullaways, the blow-hole conclusions are valid over the majority of the model length, but end effects mute the sensitivity to operational terms. However, in general, the blow-hole results are smoother than corresponding pullaway data.

GENERAL RESULTS

Larger geometric defects cause larger static pressure and larger heating, at the closure o-ring region. Velocity trends are not generally so straight-forward. Variations in assembly tolerences do not affect flowfields or heating.

Operational parameters affect closure o-ring flowfields and heating as might be expected. Increases in Re or velocity increase the heating.

NOMENCLATURE

d/d	Liner exit-to-entrance diameter ratio	Subscripts
h	Heat transfer coefficient	
M	Mach No.	b Bore
P	Pressure	g Gap
q	Heat rate	o Stagnation
Re	Reynolds No.	s Static
RSRM	Redesigned SRM	T Total
SRM	Solid Rocket Motor	W Wall
T	Temperature	
V	Velocity	
X	Axial distance (along bore length)	
Y	Vertical distance (along slot depth)	

REFERENCES

1. McAnally, James V., and Leroy M. Hair, "2-D SRM Nozzle-to-Case Joint Test Data Report", Huntsville Sciences Corp. Report HSC-SRB-001, 24 August 1988.

2. Congleston, D.W., and C.H. Wright, "Space Shuttle SRM Cold Flow Tests", Morton Thiokol Report TWR-10604, 31 - July 1975.

3. Crain, William K., and Carl D. Engel, "SRM Field Joint Cold Flow Test Data Report (SRM D MSFC Test 15)", REMTECH Inc. Report RTR-158-03, December 1986.

4. Ghosh, Ashoke, and R. Harold Whitesides, "Subscale Cold Flow Test, Aft Field Joint (MSFC Test 21, Phase II)", SRS Technologies System Technology Division Report SRS/STD-TR88-13, 13 November 87.

Report SRS/STD-TR88-13, 13 November 87.

5. Ramachandran, N., James V. McAnally, and Leroy M. Hair, "Characterization of the Flow and Thermal Fields in the Shuttle SRM Nozzle-to-Case Joint", to be published at ASME Heat Transfer Conference, June 1989, Philadelphia, PA.
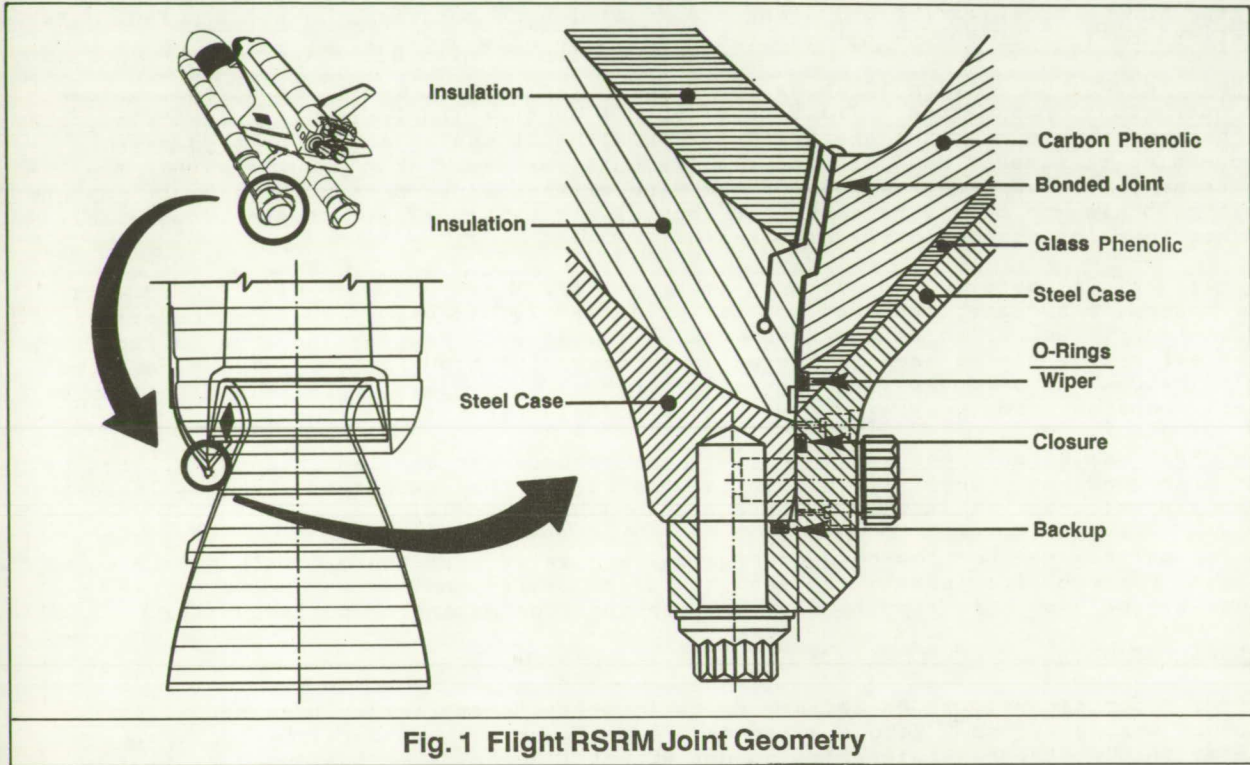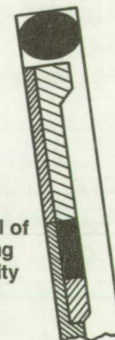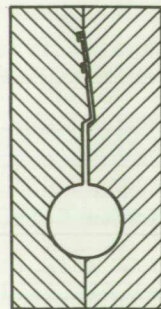

Labels: Insulation, Insulation, Steel Case, Carbon Phenolic, Bonded Joint, Glass Phenolic, Steel Case, O-Rings, Wiper, Closure, Backup

Fig. 1 Flight RSRM Joint Geometry

TABLE I. TEST CONDITIONS
(Dimensions in inches)

Id.	WIDTH	MACH NO.	LINER d/d RATIO	ASSY. TOLS.
PULLAWAY	0.100 (Vented)	0.03	.5	Sched. A
		0.07	.5 .6 .7 .8 .9 1.0	Nominal
		0.15	.8	Sched. A
			1.0	Nominal
	0.030	0.7,0.15	.8	Nominal
		0.10	.6 .7 .9 1.0	Nominal
			.8	Sched. A
	0.010	0.10	.8	Sched. A
BLOW-HOLE	LENGTH			
	4.0	0.7,0.15	.8	Nominal
		0.10	.6 .7 .9 1.0	Nominal
			.8	Sched. A
	0.5	0.10	.8	Sched. A

ASSY. TOLS.--
(See Fig.4)
Note that Sched. A
includes Sched. B,
& Sched. B incls Nom.

a	c	
.002	.050	
.002	.042	
.006	.046	(Nom.) Sched. B, Sched. A
.010	.050	
.010	.042	

MACH NO.	Re/ft at Po=60 psia	dP/dX ÷ Po (1/in.) at d/d=				
		0.5	0.6	0.7	0.8	0.9
0.03	0.907 M	.00016	.00008			
0.05	1.511 M	.00044	.00021	.00011	.00007	
0.07	2.115 M	.00090	.00042	.00022	.00013	.00008
0.10	3.022 M.		.00077	.00046	.00026	.00016
0.15	4.533 M.				.00060	.00037
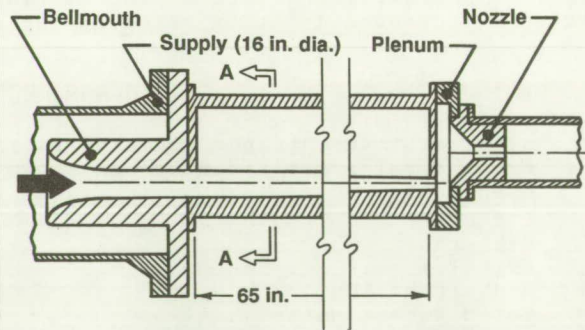
Labels: Bellmouth, Supply (16 in. dia.), Plenum, Nozzle, A, A, 65 in., Section A-A, Detail of O-Ring Vicinity

Fig. 2 Basic Model Geometry

a. Pullaways

.010" .020" .030" .100"
                        (Vented)

b. Blow-holes

0.5 - 4.0"
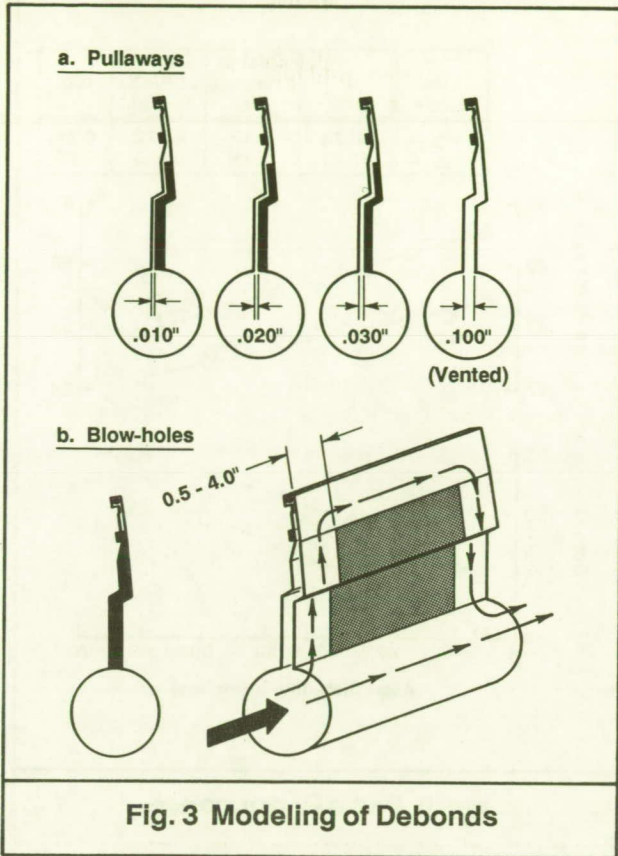
Fig. 3 Modeling of Debonds

Dimensions in inches

.040 Fixed

.004-
.008

a. Wiper < Lands   b. Wiper > Lands

a
b
c

	Min.	Nom.	Max.
a	.002	.006	.010
b	.042	.046	.050
c	.042	.046	.050

c. Wiper = Lands
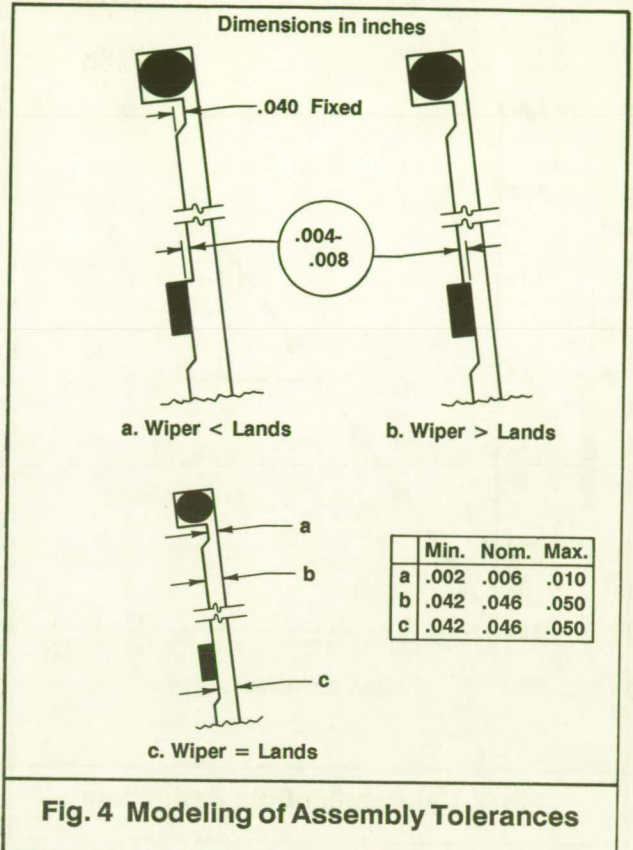
Fig. 4 Modeling of Assembly Tolerances

Dimensions in inches

X

"P" Planes (6)

A   E

"h" Planes (5)

Pressure

● - Static
T - Total

Heat Rate

■ - Calor-
    imeter

Y

●, T -

"P" Planes (6)   "h" Planes (5)

Fig. 5 Instrumentation

Air at 520°R

P_c = 665-915 psia
at 6000°R

$Re/L =$

4×10^6/ft

3

2

1

T = 5000-6000°R
at 700 psia

4000°R

Bore Mach No., M_b

.20

.15

.10

.05

0

20   30   40   50   60

Pressure (psia)
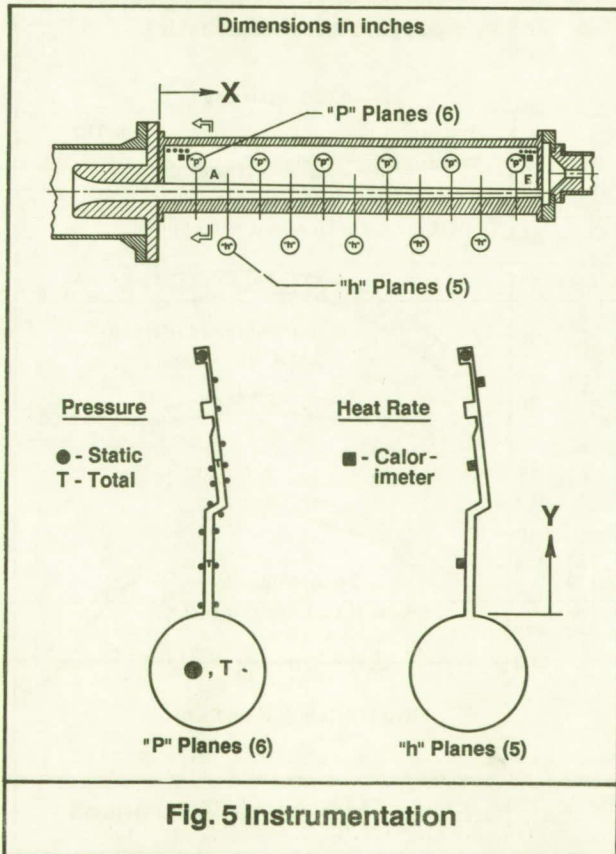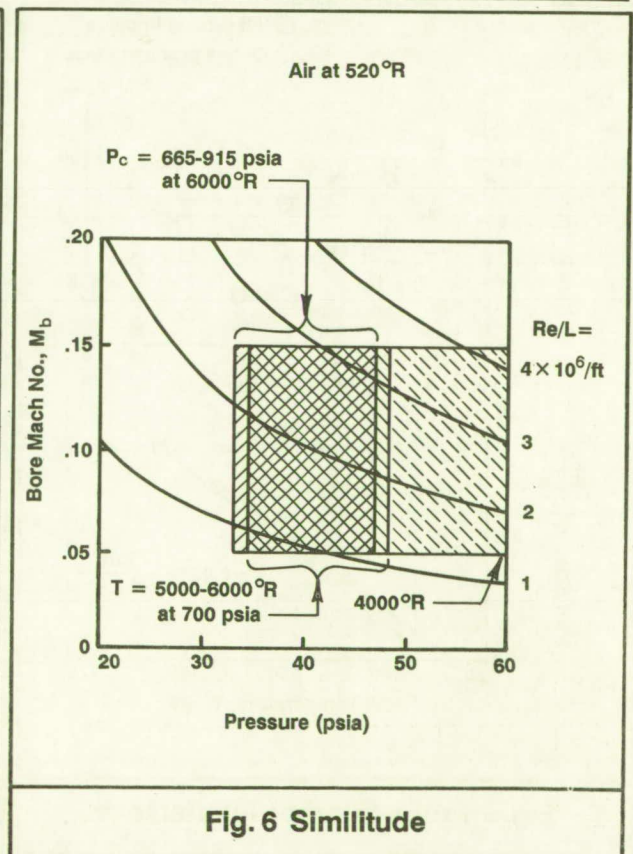
Fig. 6 Similitude
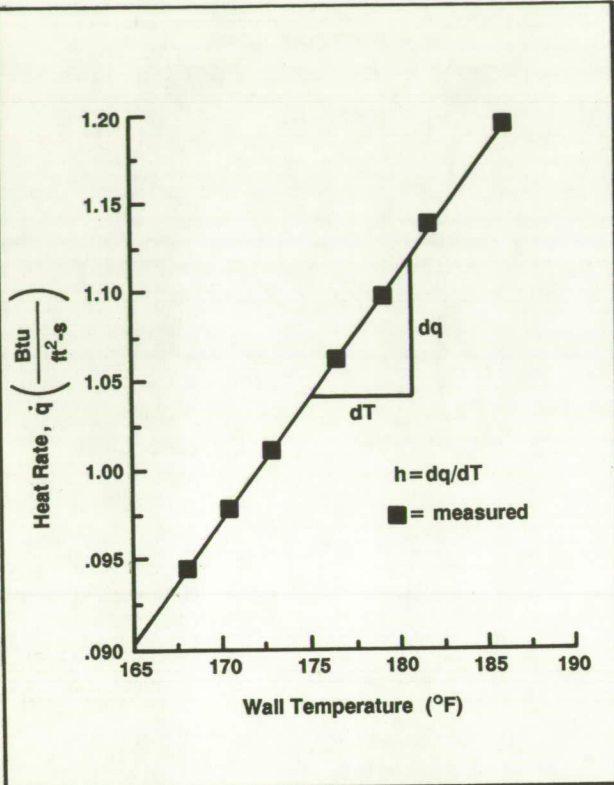
Fig. 7 Calorimeter Data Reduction

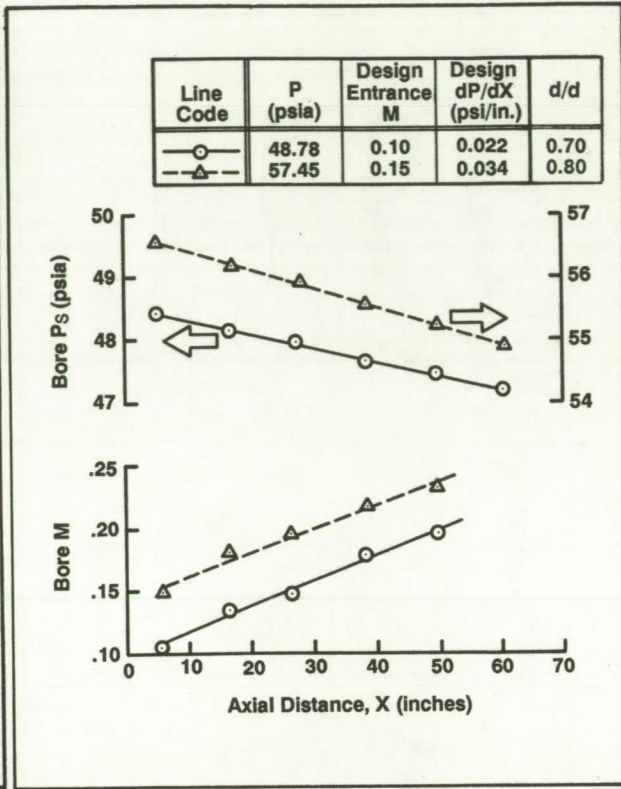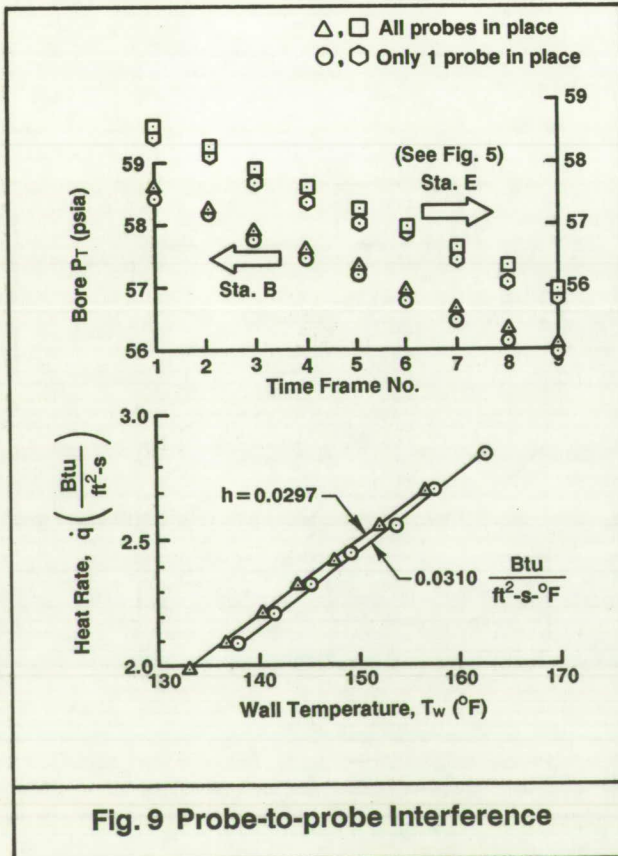| Line Code	P (psia)	Design Entrance M	Design dP/dX (psi/in.)	d/d
◯	48.78	0.10	0.022	0.70
△	57.45	0.15	0.034	0.80

Fig. 8 Basic Performance
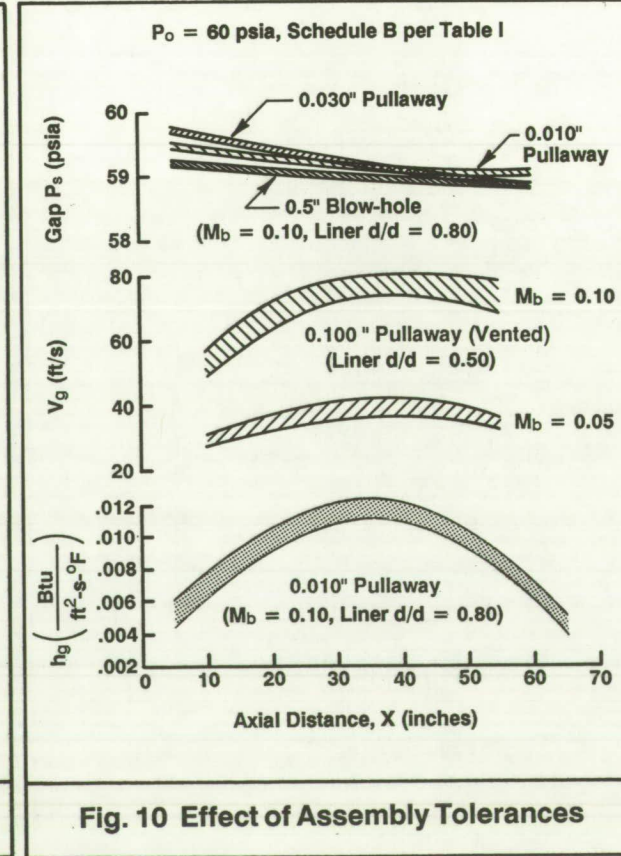

Fig. 9 Probe-to-probe Interference
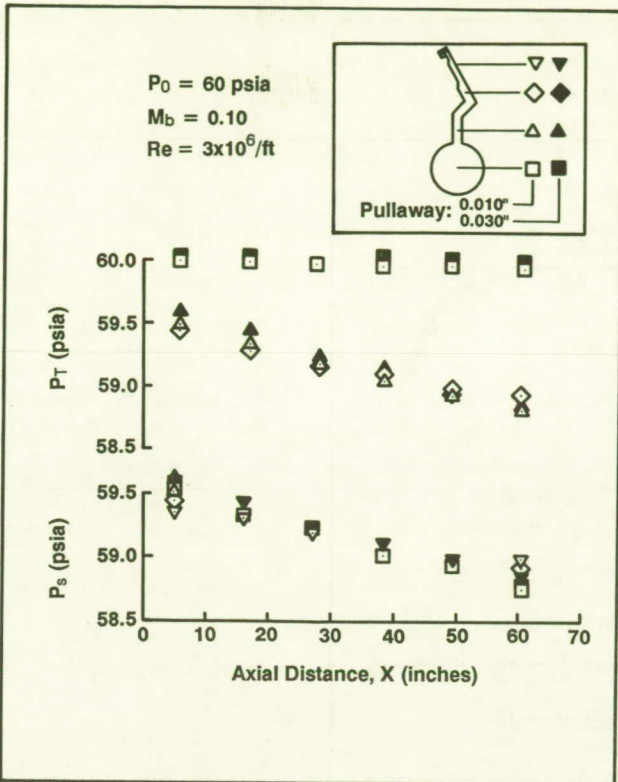

Fig. 10 Effect of Assembly Tolerances
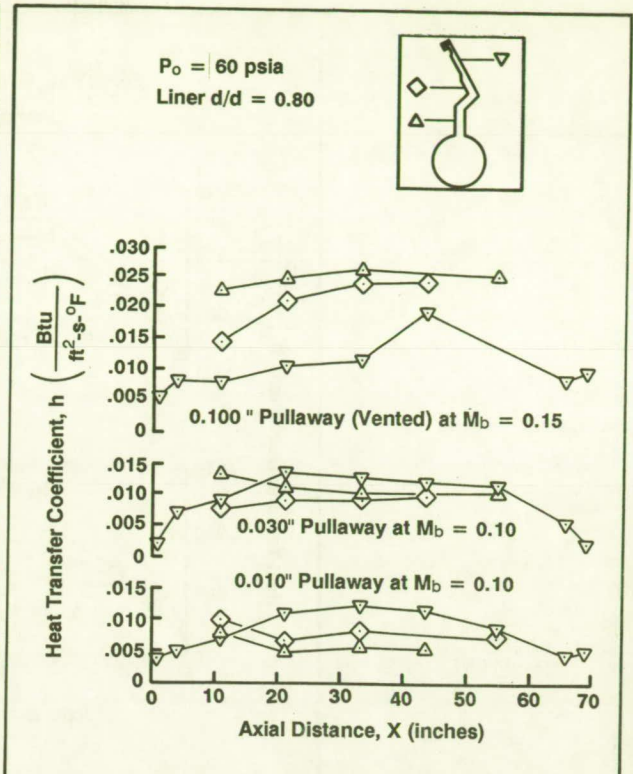
Fig. 11 Pressure Is Constant Along Gap For Pullaway Debonds
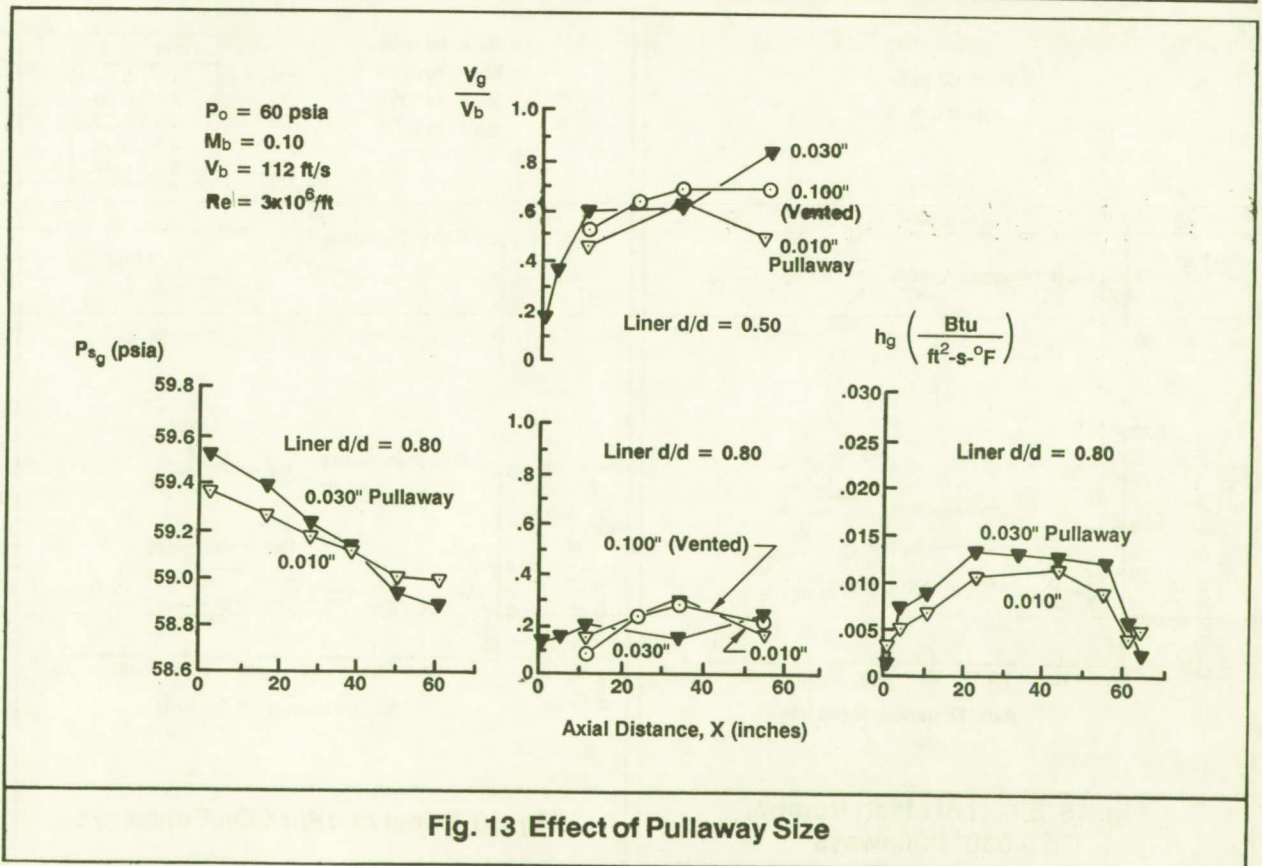

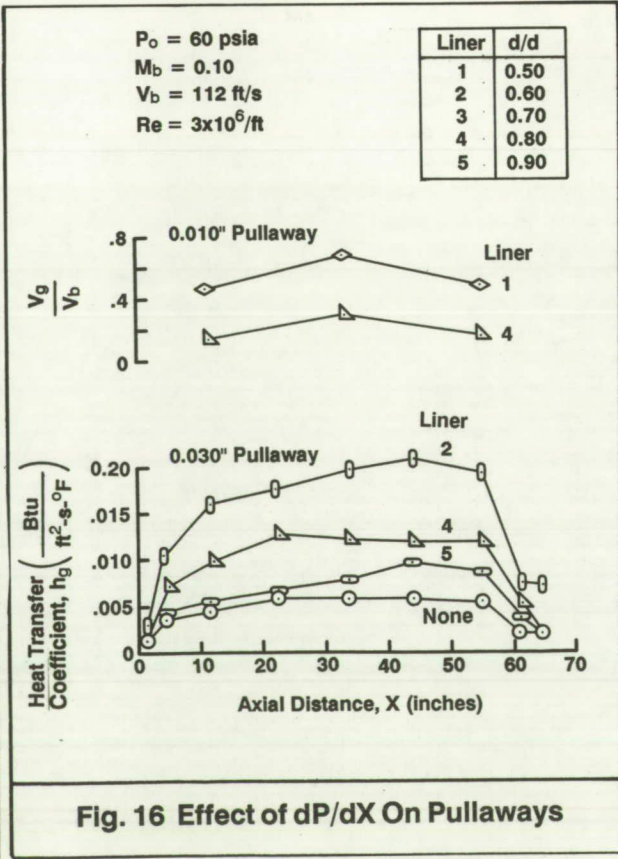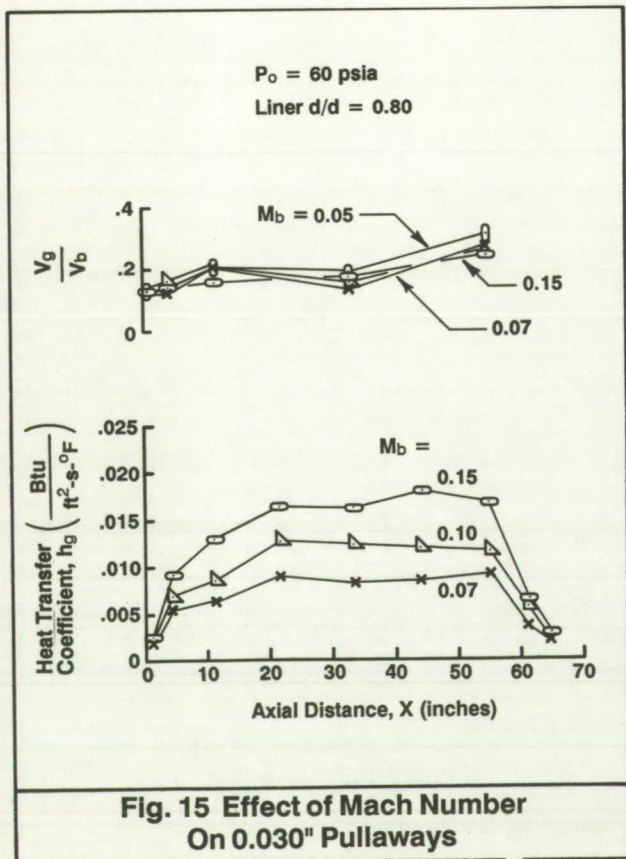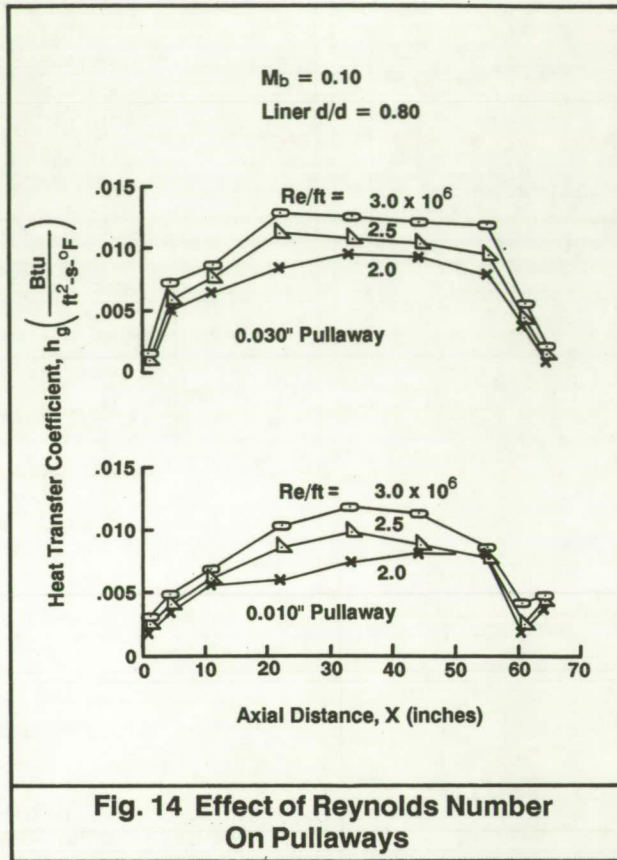**Fig. 12 Heat Transfer Coefficient Varies Along Gap For Pullaway Debonds**

Fig. 13 Effect of Pullaway Size

Fig. 14 Effect of Reynolds Number On Pullaways

$M_b = 0.10$

Liner d/d = 0.80

Heat Transfer Coefficient, $h_g \left(\dfrac{Btu}{ft^2\text{-}s\text{-}{}^\circ F} \right)$

Re/ft = 3.0×10^6

2.5

2.0

0.030" Pullaway

Re/ft = 3.0×10^6

2.5

2.0

0.010" Pullaway

Axial Distance, X (inches)

Fig. 15 Effect of Mach Number On 0.030" Pullaways

$P_o = 60$ psia

Liner d/d = 0.80

$M_b = 0.05$

0.15

0.07

$\dfrac{V_g}{V_b}$

$M_b =$ 0.15

0.10

0.07

Heat Transfer Coefficient, $h_g \left(\dfrac{Btu}{ft^2\text{-}s\text{-}{}^\circ F} \right)$

Axial Distance, X (inches)

Fig. 16 Effect of dP/dX On Pullaways

$P_o = 60$ psia
$M_b = 0.10$
$V_b = 112$ ft/s
$Re = 3\times10^6$/ft

Liner	d/d
1	0.50
2	0.60
3	0.70
4	0.80
5	0.90

0.010" Pullaway

Liner

1

4

$\dfrac{V_g}{V_b}$

Liner

0.030" Pullaway

2

4

5

None

Heat Transfer Coefficient, $h_g \left(\dfrac{Btu}{ft^2\text{-}s\text{-}{}^\circ F} \right)$

Axial Distance, X (inches)

Fig. 17 Effect of Blow-hole Size

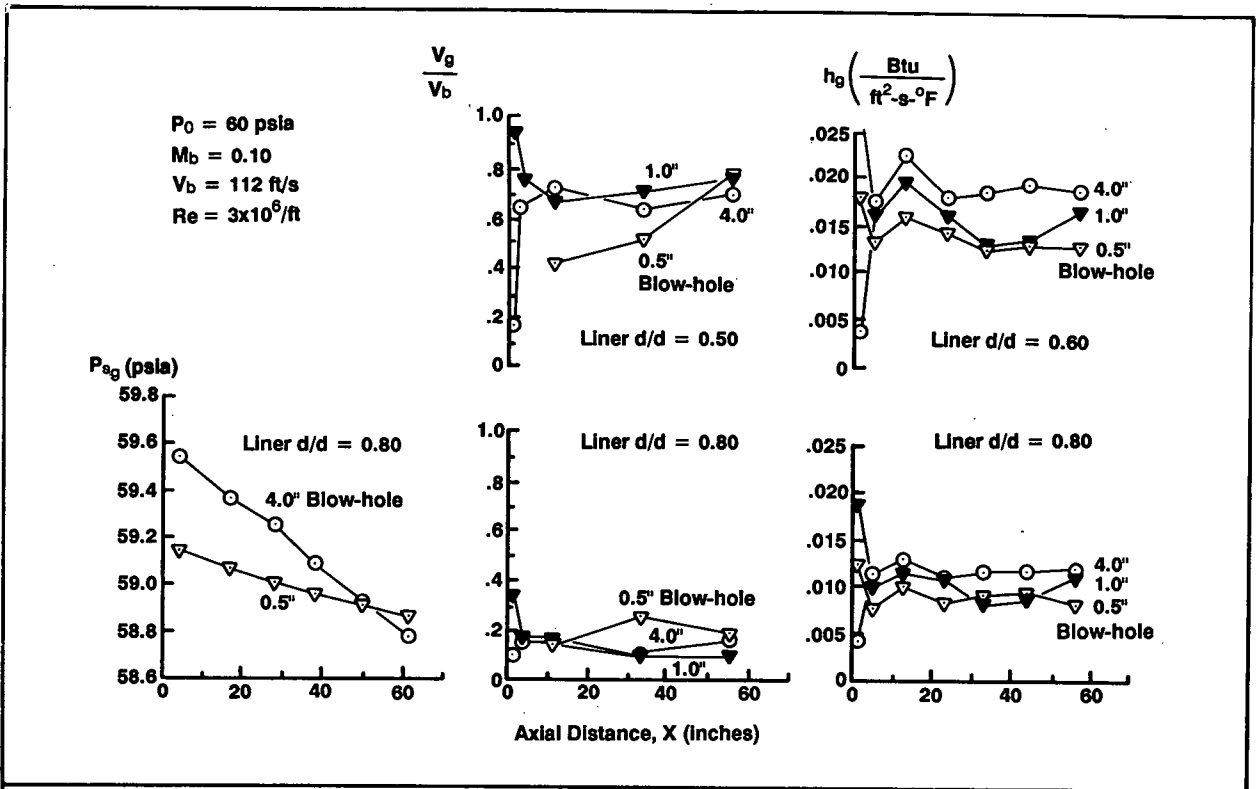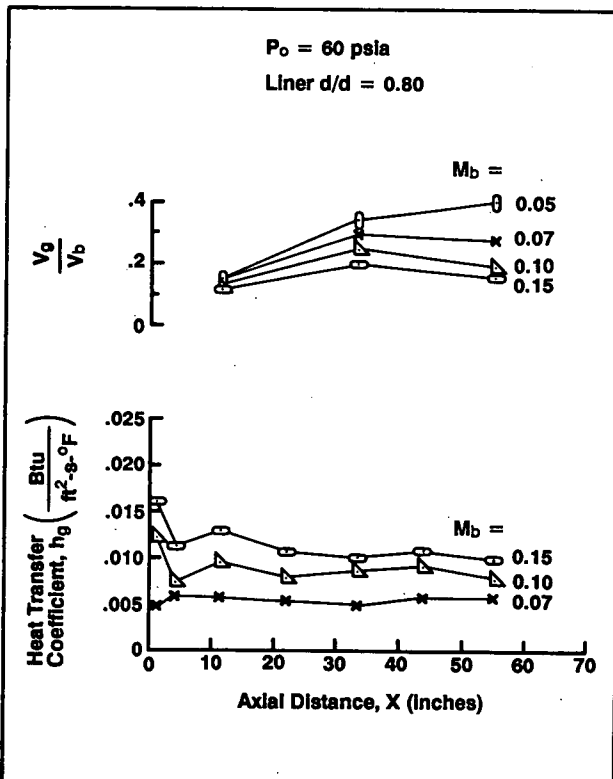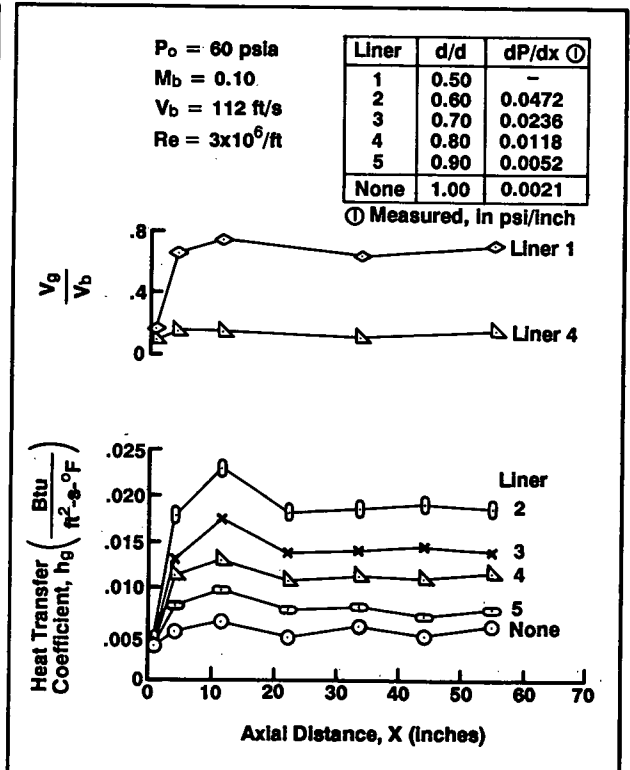**Fig. 18 Effect of Mach Number On 0.50" Blow-holes**

Fig. 19 Effect of dP/dX On 4.00" Blow-holes